eTransportation 7 (2021) 100094

Contents lists available at ScienceDirect

eTransportation

journal homepage: www.journals.elsevier.com/etransportation

An adaptive PMP-based model predictive energy management strategy for fuel cell hybrid railway vehicles☆

Kai Deng [a, *], Hujun Peng [a], Steffen Dirkes [b], Jonas Gottschalk [b], Cem Ünlübayir [c], Andreas Thul [a], Lars Löwenstein [d], Stefan Pischinger [b], Kay Hameyer [a]

[a] Institute of Electrical Machines (IEM), RWTH Aachen University, Germany
[b] Institute for Combustion Engines (VKA), RWTH Aachen University, Germany
[c] Chair for Electrochemical Energy Conversion and Storage Systems, Institute for Power Electronics and Electrical Drives (ISEA), RWTH Aachen University, Aachen, Germany
[d] Siemens Mobility GmbH, Vienna, Austria

ARTICLE INFO

Article history:
Received 28 July 2020
Received in revised form
14 November 2020
Accepted 23 November 2020
Available online 27 November 2020

Keywords:
Energy management
Fuel cell hybrid trains
Model predictive control (MPC)
Pontryagin's minimum principle (PMP)

ABSTRACT

In order to achieve ecological driving without pollutant emissions on non-electrified rail tracks, the focus is on the development of railway vehicles powered by fuel cell and battery systems. A key issue is to reduce hydrogen consumption while maintaining the battery's state of charge (SoC). In that context, this paper proposes a new casual energy management strategy based on Pontryagin's Minimum Principle (PMP) within the framework of Model Predictive Control (MPC). The entire energy management problem is formulated by solving a cost function in the prediction horizon, different from the typical one found in other work using model predictive control to realize energy management. The main advantage of this strategy is that by introducing the PMP's co-state, which is adaptively evaluated using average power estimation and actual SoC, into the cost function, a predicted optimal SoC trajectory is no longer required within the framework of MPC. Therefore, the strategy does not require complete information on the rail track and behaves casually. In addition, the dynamic of the fuel cell power is considered by introducing a tuning factor into the cost function, which benefits the service life of fuel cells. The proposed strategy is tested and validated in a realistic driving cycle by a hardware-in-the-loop (HiL) test bench at the Center for Mobile Propulsion (CMP) of RWTH Aachen University. The simulation results show an optimum close to the offline PMP results and up to 12.1% hydrogen savings compared to a typical MPC strategy using constant SoC reference. The HiL results demonstrate the real-time capability of the proposed strategy and show the excellent fuel economy with merely 2.7% more hydrogen consumption than the global optimum result.

1. Introduction

1.1. Background

In response to climate change and the need for rapid and continuous decarbonization of the railway transportation system, new technologies are taken into consideration. The use of electric multiple units (EMU) with hydrogen-powered fuel cells is an exciting and promising alternative. As a zero-emission technology in railway transportation, fuel cells using hydrogen energy are fully capable of achieving goals of reducing greenhouse gases, air pollution, and noises. Especially in long-distance and high-power use cases, it is expected that fuel cell technology can play an increasingly important role in the railway sector [1]. For multiple units in Europe, fuel cell rail vehicles could potentially replace 30% of diesel vehicles by 2030 [2]. In particular, around 40% of the German rail network is not electrified [3]. The overhead catenary construction is cost-intensive, uneconomic, and inefficient on sections of the rail track with low traffic e.g. in rural areas. So far, many efforts have been devoted to research, manufacture, and commercialization of fuel cell trains. A milestone was set in September

☆ This work is funded by the German Federal Ministry of Transport and Digital Infrastructure (BMVi) under the National Innovation Program Hydrogen and Fuel Cell Technology (NIP) with the funding numbers of 03B10502B and 03B10502B2. The authors gratefully acknowledge the support by Siemens AG and NIP.

* Corresponding author.
E-mail address: kai.deng@iem.rwth-aachen.de (K. Deng).

https://doi.org/10.1016/j.etran.2020.100094
2590-1168/

2018, the world's first commercial fuel cell regional train was put into service in Lower Saxony, Germany by Alstom S.A [4]. In collaboration with RWTH Aachen University, Siemens and Ballard are developing a Fuel Cell Electric Multiple Unit (FC-EMU) with highly dynamic battery systems based on the Mireo platform, which is planned to go into operation in 2021 [5]. This paper focuses on the energy management strategy of Siemens FC-EMU.

1.2. Literature review

Fuel cell hybrid railway vehicles are complex electromechanical systems. The power flow of a hybrid system ties to the configuration and power distribution in the driveline. Accordingly, the core issue is to formulate energy management strategies to achieve long-term stable driving for regional rail transport without external charging, while improving potential fuel economy and component lifetime. Various energy management strategies have been investigated in the last decades and can be classified into two categories: rule-based strategies and optimization-based strategies [6,7].

Rule-based strategies, including deterministic and fuzzy logic, are usually based on rules derived from human expertise, heuristic, or mathematical models without former information on the driving cycle [8,9]. This type of method is not sensitive to driving conditions, requires a low computational effort, and is simple to implement. However, the rules are challenging to define, and there is no guarantee that they are optimal [6]. To improve the rule-based strategy's performance, many optimization methods such as dynamic programming (DP) are devoted to finding the proper thresholds and parameters [10,11]. Nevertheless, these optimized thresholds and parameters rely on specific driving cycles, which restrict the casualness.

As for the optimization-based strategies, the whole energy management problem is formulated to minimize operating costs over a considered time period. Two types of strategies can be subdivided: global optimization and real-time optimization [7]. Concerning the global optimization methods, DP and Pontryagin's Minimum Principle (PMP) are commonly used. Based on the Bellman's optimal principle [12], DP simplifies a complex problem by recursively decomposing it into many small sub-problems. Some methods like two-dimensional dynamic programming are investigated to improve the computing efficiency [13]. However, the knowledge of the driving cycle must be given in advance to obtain the global optimum. Furthermore, DP is troubled by the "explosion of dimensions", and because of its computational consumption and the need for a large amount of memory, it can only be implemented offline and used as a benchmark reference. In contrast, the PMP-based method does not require a lot of computational effort. It determines the optimal power flow by obtaining the instantaneous minimum value of the Hamiltonian function at every instant. Thereby, an often-used method is the shooting method, which searches the initial values to fulfill the problem's boundary conditions [14]. Thus, the global optimization of PMP is also bounded to driving cycles and is used as offline optimization.

As real-time optimization, instantaneous optimization strategies, including equivalent consumption minimization strategy (ECMS) and the model predictive control strategy (MPC), are prominent. Generally for ECMS, as a form of PMP strategy [15], an equivalent cost function is set to transform a global optimization problem to a local one. The core issue is to find the proper equivalent factor, which can in the best way transfer the electric power consumption into fuel consumption. One basic method is to obtain a fixed equivalent factor by DP with the known driving cycle [16]. In order to make ECMS not sensitive to the driving cycle, different adaptive ECMS can be found in the literature. In Ref. [17], the authors use feedback control to apply the correction term to the offline optimized factor. In Ref. [15], the calculation for the value range of the optimal equivalent factor is improved. In Ref. [18], a driving style recognition is offline trained and implemented in ECMS. However, they still need one optimized reference like the battery's state of charge (SoC), which is derived offline or requires a significant effort to train a tool for driving style recognition.

Moreover, taking future information into consideration, MPC is another powerful method for real-time optimization. It takes the current state as the initial state, predicts the states and model outputs over the predicted horizon, optimizes each sampling moment and finally applies the first optimal control sequence [19]. The success of MPC is mainly due to its capability to manage strict constraints on control and state directly and effectively. Furthermore, it solves optimization problems at every time step, which allows the controller to adapt to actual operating conditions. In Ref. [20], a stochastic MPC based on the PMP is proposed, which uses a shooting method to determine the co-state according to a dynamically tuned reference SoC, and realizes the power distribution by minimizing the Hamiltonian function. In Ref. [21], a high-level MPC controller provides a battery energy target for a lower layer that uses DP and PMP to calculate the optimal power distribution. In Ref. [22], a multi-level MPC is proposed, based on a method that suggests a reference SoC trajectory. In Ref. [23], an adaptive SoC reference generator is built and quadratic programming is used to solve MPC-based energy management. For the application of fuel cell hybrid systems in Ref. [24,25], the objective functions include the degradation costs of fuel cells, and a SoC reference is used to achieve battery's charge-sustaining. Overall, the performance of the MPC depends highly on the predicted reference values such as SoC, which should be well designed.

In recent years, data-driven approaches, such as neural networks and machine learning [26,27], have been used in energy management system. With the help of environmental information interaction, these methods can be utilized to predict future conditions, which are involved in MPC to achieve better performance [28]. Alternatively, control strategies can be trained offline based on the collected data [29]. However, data-driven methods rely on the collected data and require high training effort.

1.3. Motivation

Due to the long-distance, regional railway transport without an overhead catenary charging system, the studied fuel cell railway vehicle is designed to drive in a battery's charge-sustaining mode. As a buffer unit, the traction battery provides dynamic power, while the fuel cell system covers the demand of average power. The energy management has to consider the current state constraints and adjust the optimum control in real-time. Among the literature [19], MPC is a promising approach to handle this issue. Nevertheless, to reach the control goals for charge-sustaining of battery, the deviation of SoC from the reference value is often weighted in the cost function [30–32]. A fixed reference value can guarantee casualness yet no optimality [24,25]. However, an offline obtained reference restricts the control strategy to the driving cycle. Furthermore, an online estimated reference depends on the estimation accuracy, which is also challenging to ensure optimality [20–23].

1.4. Main contributions

In order to overcome the shortcomings mentioned above, this paper proposes a novel PMP-based MPC to solve the problem of optimum energy management for fuel cell railway vehicles. The main contributions are highlighted as follows: (1) Unlike other MPC-based strategies, the proposed method does not require a preview of the complete driving cycle or the generation of SoC

reference trajectory. An online adaptively estimated co-state, as defined in the PMP method, is introduced in MPC's cost function to ensure optimum power distribution and charge-sustaining mode. (2) A dynamic battery model with three R–C elements is integrated into MPC. (3) The proposed method is tested and validated by a hardware-in-the-loop (HiL) test with high power fuel cell and battery systems.

1.5. Organization of the paper

In Section 2, the modeling of the driveline for investigating energy management is presented. In Section 3, the framework of PMP-based MPC is introduced and the adaptive estimation of co-state is given. Section 4 approves the fuel economy of the proposed strategy, as compared to the results of offline PMP-based strategies and typical MPC strategies. Meanwhile, the analyses of the parameters in the cost function are discussed. Then in Section 5, the setup of HiL test bench at the Center for Mobile Propulsion (CMP) of RWTH Aachen University and the test results are given. Finally, Section 6 summarizes the conclusions.

2. Modeling of the driveline

The modeling of the fuel cell railway vehicle considers the half train due to the symmetrical vehicle configuration. For analyzing the energy efficiency of the powertrain, the vehicle dynamics and battery dynamics are considered, and the power losses in the drivetrain, electric motor, DC/DC converters, and the power consumption of auxiliaries are determined based on look-up tables. Fig. 1 shows the topology of the powertrain. In the following subsections, the modeling of vehicle dynamics, fuel cell system, and battery system are briefly introduced. Other detailed component models can be found in our previous work [33].

2.1. Vehicle dynamics

A forward-simulated longitudinal dynamic railway vehicle model is set up in this work. A proportional–integral (PI) controller models the driver behavior and controls the speed tracking. Considering the traction forces and all the resistance forces, the longitudinal dynamics are described by the following equation (1):

Table 1
Parameters for vehicle dynamics.

Parameters	Symbols	Values	Units
Vehicle mass (including 120 passengers)	m	60,000	kg
Gravitational acceleration	g	9.81	m/s^2
Rolling resistance coefficient	μ_r	0.0015	–
Density of air	ρ_{air}	1.4	kg/m^3
Aerodynamic coefficient	C_d	0.15	–
Front area	A_f	10	m^2

$$m\cdot\frac{dv}{dt} = F_x - \mu_r mg\cos(\varphi) - \frac{1}{2}\rho_{air}C_d A_f v^2 - mg\sin(\varphi) - F_b, \quad (1)$$

where m is the vehicle mass, v is the speed, F_x is the traction force on wheels, μ_r is the coefficient of rolling resistance, ρ_{air} is the density of air, C_d is the aerodynamic coefficient, g is the gravitational acceleration, A_f is the front area, φ is the angle of slope, and F_b is the mechanical brake force. The related parameters are shown in Table 1 [34].

2.2. Fuel cell system

As an energy source providing average power, a high power polymer electrolyte membrane (PEM) fuel cell system is used in this railway vehicle. The fuel cell system with 200 kW rated net power has an internal DC/DC converter to control the power output. For the study of energy management, the fuel cell system is modeled stationarily without considering dynamic electrochemical mechanisms or degradation processes. The hydrogen consumption curve is shown in Fig. 2, which is fitted by a 5th order polynomial function related to fuel cell power:

$$\overline{m}_{H_2} = f(P_{fc}). \quad (2)$$

2.3. Battery system

The battery has a total capacity of 200 kWh and a rated voltage of 850 V, where real measurement data from pulse tests and electrochemical impedance spectroscopy (EIS) are used to parameterize the model. This battery system has three branches and is modeled based on cell modeling. According to the measurement results, three R–C elements can accurately approximate the real

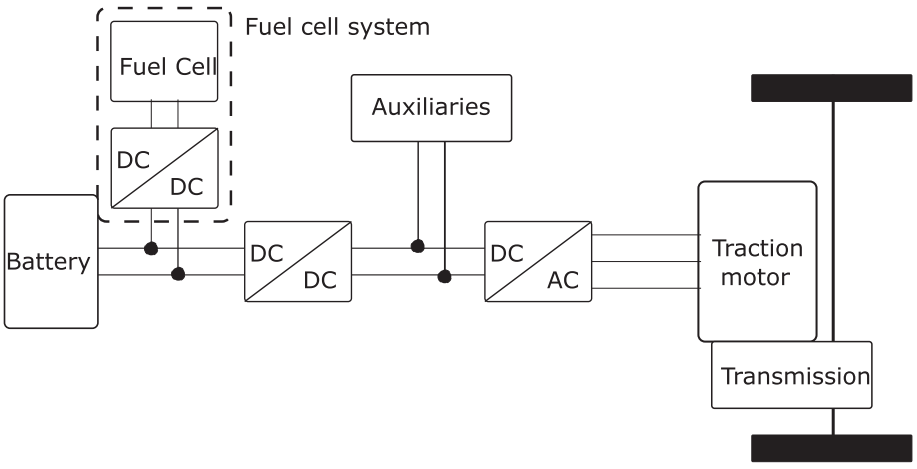

Fig. 1. System configuration of the studied fuel cell hybrid train.

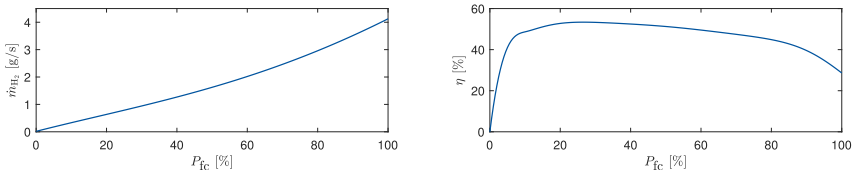

(a) (b)

Fig. 2. Fuel cell system: (a) Specific consumption curve, (b) Efficiency of system.

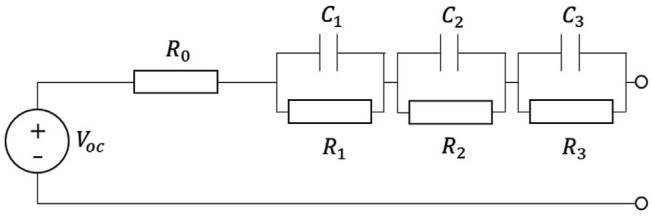

Fig. 3. Battery's equivalent circuit with three R–C elements.

dynamic performance of the battery. Fig. 3 shows the battery's equivalent circuit, where the parameters of open circuit voltage V_{oc} and resistances are shown in Fig. 4. Because of a well adjusted active cooling, the battery is assumed to be ideally controlled at 25 °C. Considered the three R–C elements, following equations describe the battery dynamics:

$$\overline{SoC} = -\frac{I_{bat}}{Q_{bat}}, \tag{3}$$

$$I_{bat} = \frac{V_{oc} - \sum_{i=1}^{3} V_i}{2R_0} - \sqrt{\left(\frac{V_{oc} - \sum_{i=1}^{3} V_i}{2R_0}\right)^2 - \frac{P_{bat}}{R_0}}, \tag{4}$$

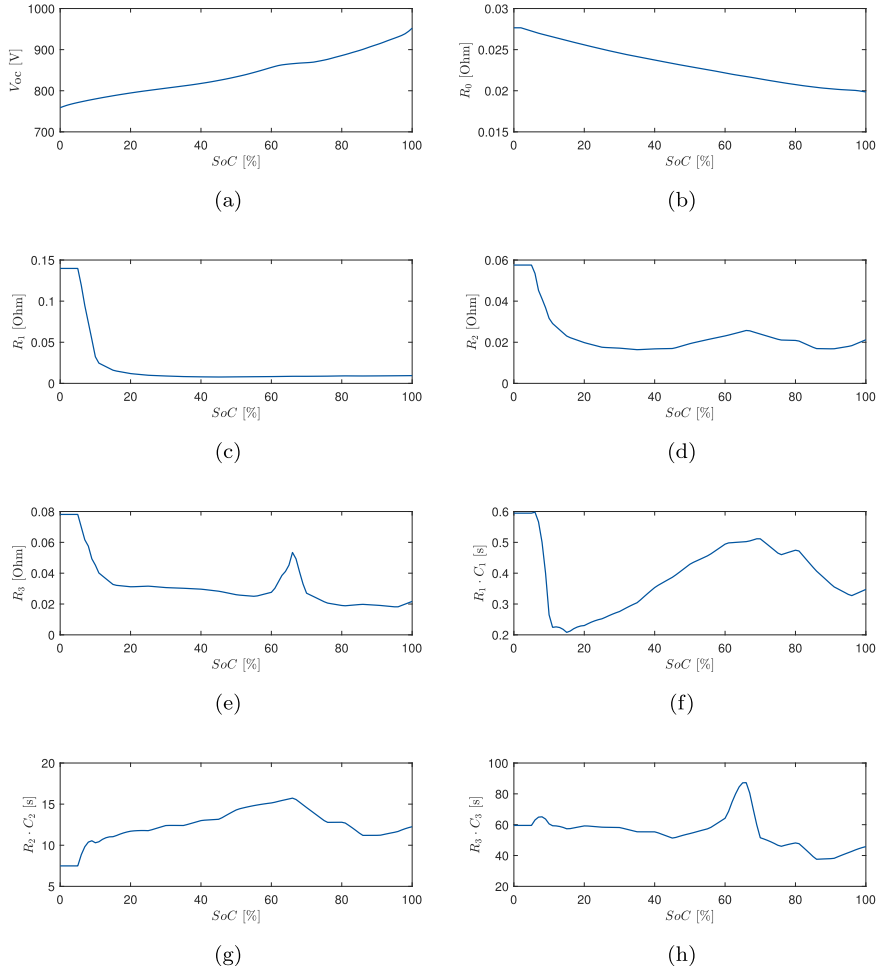

(a) (b) (c) (d) (e) (f) (g) (h)

Fig. 4. Parameters of the battery's equivalent circuit at 25 °C: (a) V_{oc} in V, (b) R_0 in Ω, (c) R_1 in Ω, (d) R_2 in Ω, (e) R_3 in Ω, (f) Time constant $R_1 \cdot C_1$ in second, (g) Time constant $R_2 \cdot C_2$ in second, (h) Time constant $R_3 \cdot C_3$ in second.

$$\overline{V}_i = \frac{I_{\text{bat}}}{C_i} - \frac{V_i}{R_i \cdot C_i}, \quad i = 1,2,3, \tag{5}$$

where Q_{bat} is the battery capacity, I_{bat} is the battery current, R_0 is the internal ohmic resistance, R_1, R_2 and R_3 are the polarization resistances, C_1, C_2 and C_3 are the polarization capacitances, V_1, V_2 and V_3 are the voltages over the capacitances and P_{bat} is the battery power, which is the difference between the demand load power P_{dem} of the vehicle and the fuel cell power P_{fc}:

$$P_{\text{bat}} = P_{\text{dem}} - P_{\text{fc}}. \tag{6}$$

Thereby, P_{dem} is controlled by the driver and P_{fc} is controlled by the energy management controller. Since a source side DCDC converter is used to control the voltage of the DC link, the battery system fills the difference between P_{dem} and P_{fc}. In this way, the load power is distributed. It should be noted that the power split ratio is not used in the following energy management design. Instead, the control variable P_{fc} is chosen, which has the same functionality on the power distribution.

3. PMP-based MPC

The focus of this work is on optimum decisions of power distribution between the battery and fuel cell system for hybrid railway vehicles without external charging. The energy management module determines the desired power output of the fuel cell system according to the power demand from the driver and the system. Due to the dynamic nature of power demand, this is a dynamic decision-making problem. The goal is to achieve better fuel economy and sustaining the charge of the battery while ensuring no constraint is violated. For this constrained nonlinear dynamic optimization problem, the need for an approach based on real-time optimization motivates us to use MPC.

3.1. PMP-based MPC formulation

It is assumed that by using the PI controller to control the vehicle speed, its value ideally follows the reference speed trajectory. Therefore, the vehicle speed dynamic will not be considered in the framework of MPC, and merely the dynamics related to the battery system are included. Then, a linear time-varying (LTV) model based on the equations (2)–(6) is introduced. In order to linearize the system model, battery parameters in Fig. 4 related to the battery's SoC at 25 °C are fitted by piecewise polynomial functions. The nonlinear continuous model is linearized around the operation point by the Jacobian and the resulted state-space representation is:

$$\begin{cases} \overline{\boldsymbol{x}} = \boldsymbol{f}(\boldsymbol{x},\boldsymbol{u},\boldsymbol{v}) = \boldsymbol{A}^c\boldsymbol{x} + \boldsymbol{B}_u^c\boldsymbol{u} + \boldsymbol{B}_v^c\boldsymbol{v} + \boldsymbol{F}^c, \\ \boldsymbol{y} = \boldsymbol{g}(\boldsymbol{x},\boldsymbol{u},\boldsymbol{v}) = \boldsymbol{C}^c\boldsymbol{x} + \boldsymbol{D}_u^c\boldsymbol{u} + \boldsymbol{D}_v^c\boldsymbol{v} + \boldsymbol{G}^c, \end{cases} \tag{7}$$

where

$$\boldsymbol{x} = \begin{bmatrix} SoC \\ V_1 \\ V_2 \\ V_3 \end{bmatrix}, \quad \boldsymbol{u} = [P_{\text{fc}}], \quad \boldsymbol{v} = [P_{\text{dem}}], \quad \boldsymbol{y} = \begin{bmatrix} \overline{SoC} \\ \overline{m}_{\text{H}_2} \\ SoC \end{bmatrix}, \tag{8}$$

$$\begin{aligned} \boldsymbol{A}^c &= \left(\frac{\partial \boldsymbol{f}}{\partial \boldsymbol{x}}\right)_{(\boldsymbol{x}_0,\boldsymbol{u}_0,\boldsymbol{v}_0)}; \boldsymbol{B}_u^c = \left(\frac{\partial \boldsymbol{f}}{\partial \boldsymbol{u}}\right)_{(\boldsymbol{x}_0,\boldsymbol{u}_0,\boldsymbol{v}_0)} \\ \boldsymbol{B}_v^c &= \left(\frac{\partial \boldsymbol{f}}{\partial \boldsymbol{v}}\right)_{(\boldsymbol{x}_0,\boldsymbol{u}_0,\boldsymbol{v}_0)}; \boldsymbol{C}^c = \left(\frac{\partial \boldsymbol{g}}{\partial \boldsymbol{x}}\right)_{(\boldsymbol{x}_0,\boldsymbol{u}_0,\boldsymbol{v}_0)} \\ \boldsymbol{D}_u^c &= \left(\frac{\partial \boldsymbol{g}}{\partial \boldsymbol{u}}\right)_{(\boldsymbol{x}_0,\boldsymbol{u}_0,\boldsymbol{v}_0)}; \boldsymbol{D}_v^c = \left(\frac{\partial \boldsymbol{g}}{\partial \boldsymbol{v}}\right)_{(\boldsymbol{x}_0,\boldsymbol{u}_0,\boldsymbol{v}_0)} \\ \boldsymbol{F}^c &= \boldsymbol{f}(\boldsymbol{x}_0,\boldsymbol{u}_0,\boldsymbol{v}_0) - \boldsymbol{A}^c\boldsymbol{x}_0 - \boldsymbol{B}_u^c\boldsymbol{u}_0 - \boldsymbol{B}_v^c\boldsymbol{v}_0 \\ \boldsymbol{G}^c &= \boldsymbol{g}(\boldsymbol{x}_0,\boldsymbol{u}_0,\boldsymbol{v}_0) - \boldsymbol{C}^c\boldsymbol{x}_0 - \boldsymbol{D}_u^c\boldsymbol{u}_0 - \boldsymbol{D}_v^c\boldsymbol{v}_0 \end{aligned} \tag{9}$$

with the linear system matrices $\boldsymbol{A}^c$, $\boldsymbol{B}_u^c$, $\boldsymbol{B}_v^c$, $\boldsymbol{C}^c$, $\boldsymbol{D}_u^c$, $\boldsymbol{D}_v^c$, $\boldsymbol{F}^c$, $\boldsymbol{G}^c$, which are updated at each time step. In Eq. (8), $\boldsymbol{x}$ is the state vector, $\boldsymbol{u}$ is the control vector, $\boldsymbol{v}$ is the disturbance vector and $\boldsymbol{y}$ is the output vector.

As the disturbance of the system, the power demand is the sum of traction power P_{traction}, power losses along the driveline P_{loss} and the power consumption of auxiliaries P_{aux}:

$$P_{\text{dem}} = P_{\text{traction}} + P_{\text{loss}} + P_{\text{aux}}. \tag{10}$$

The future traction power depends on the speed prediction and the rail track. Because the focus of this work is on optimum power distribution for energy management, the speed and the road gradient in the prediction horizon are assumed to be ideally extracted from the navigation data system. Then, the future traction power is estimated by

$$P_{\text{traction}} = \left(m \cdot a + \mu_{\text{r}} mg\cos(\varphi) + \frac{1}{2} \cdot \rho_{\text{air}} C_{\text{d}} A_{\text{f}} v^2 + mg\sin(\varphi)\right) \cdot v, \tag{11}$$

with the vehicle acceleration $a = \frac{v((k+1)T) - v(kT)}{T}$ and the sample time T. Using the speed and traction power, the power losses along the driveline are calculated by the look-up tables, which refers to Ref. [33]. Furthermore, the power consumption of auxiliaries is assumed to be constant with 55 kW for summer and 83 kW for winter during the whole trip, which can be found in Ref. [13].

By simulating both the linearized model and the original plant model with the same initial states under the identical control and disturbance signals, the trajectories of the state and output variables are displayed in Fig. 5. The simulation runs for 10 s. The sample time of the linearized model is 1 s and the sample time of the plant model is 0.01 s. The average errors of SoC and the hydrogen mass flow are 0.01% and 1.1%, respectively. It can be pointed out, the linearized model has a small error compared to the plant model. As the linearized model is updated at each sample time, the correctness of the linearized model as the internal prediction model can be ensured.

Finally, under the MPC structure, a discrete time state space model is used, which can be discretized from (7) at every time step. Assuming constant inputs between two consecutive time steps, the following transition matrices are used: $\boldsymbol{A}^D = \exp(\boldsymbol{A}^c T)$, $\boldsymbol{B}_u^D = (\boldsymbol{A}^c)^{-1} \cdot (\exp(\boldsymbol{A}^c T) - \mathbf{I}) \cdot \boldsymbol{B}_u^c$, $\boldsymbol{B}_v^D = (\boldsymbol{A}^c)^{-1} \cdot (\exp(\boldsymbol{A}^c T) - \mathbf{I}) \cdot \boldsymbol{B}_v^c$, $\boldsymbol{F}^D = \exp(\boldsymbol{A}^c T) \cdot \boldsymbol{F}^c$, $\boldsymbol{C}^D = \boldsymbol{C}^c$, $\boldsymbol{D}_u^D = \boldsymbol{D}_u^c$, $\boldsymbol{D}_v^D = \boldsymbol{D}_v^c$ and $\boldsymbol{G}^D = \boldsymbol{G}^c$. Then, the MPC problem can be written as:

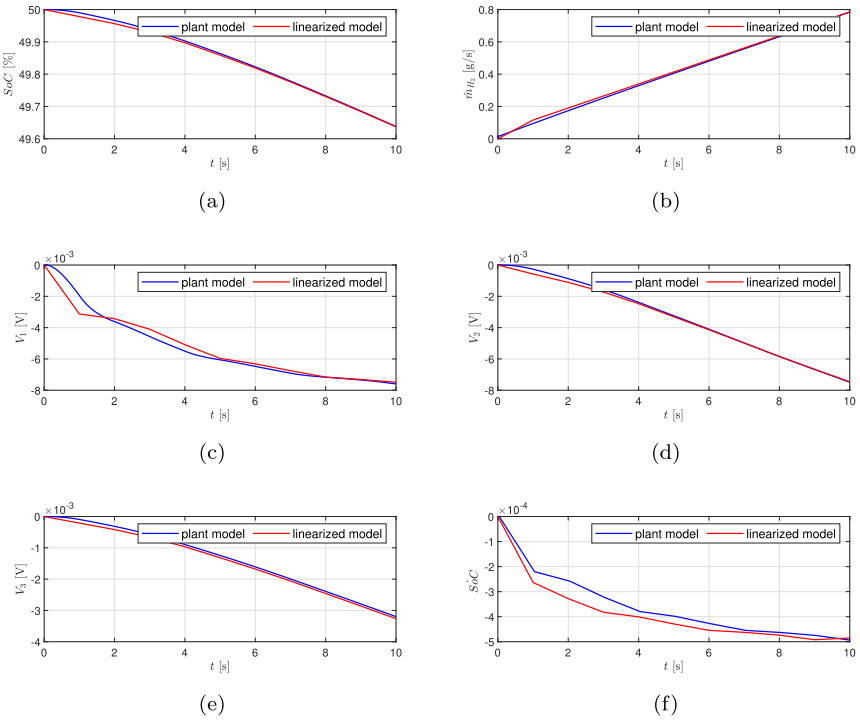

Fig. 5. Comparison between the linearized model and plant model by applying the same control and disturbance at the identical initial state: (a) *SoC* in %, (b) $\overline{m}_{H_2}$ in g/s, (c) V_1 in *V*, (d) V_2 in *V*, (e) V_3 in *V*, (f) $\overline{SoC}$.

$$\min_{\Delta u} J(\Delta u) = \underbrace{\sum_{i=0}^{N_u-1} \| \Delta u(k+i|k)\|^2_{W_{\Delta u}}}_{\text{penalty of the fuel cell power oscillation}} + \underbrace{\lambda \sum_{i=0}^{N_p} y_1(k+i+1|k)T}_{\text{battery consumption}} + \underbrace{\sum_{i=0}^{N_p} y_2(k+i+1|k)T}_{\text{hydrogen consumption}}, \quad i = 1, \cdots, N_p - 1, \tag{12}$$

subject to:

$$\begin{cases} \boldsymbol{x}(k+1) = \boldsymbol{A}^D \boldsymbol{x}(k) + \boldsymbol{B}_u^D \boldsymbol{u}(k) + \boldsymbol{B}_v^D \boldsymbol{v}(k) + \boldsymbol{F}^D, \\ \boldsymbol{y}(k) = \boldsymbol{C}^D \boldsymbol{x}(k) + \boldsymbol{D}_u^D \boldsymbol{u}(k) + \boldsymbol{D}_v^D \boldsymbol{v}(k) + \boldsymbol{G}^D, \\ \boldsymbol{x}_{min} \le \boldsymbol{x}(k+i+1|k) \le \boldsymbol{x}_{max}, \\ \boldsymbol{y}_{min} \le \boldsymbol{y}(k+i+1|k) \le \boldsymbol{y}_{max}, \\ \boldsymbol{u}_{min} \le \boldsymbol{u}(k+i|k) \le \boldsymbol{u}_{max}, \\ \Delta \boldsymbol{u}_{min} \le \Delta \boldsymbol{u}(k+i|k) \le \Delta \boldsymbol{u}_{max}, \end{cases}$$

where N_p and N_u are the prediction and control horizons, $\boldsymbol{x}(k+i+1|k)$, $\boldsymbol{y}(k+i+1|k)$, $\boldsymbol{u}(k+i|k)$, $\Delta\boldsymbol{u}(k+i|k)$ denote the prediction of the variable based on the information at time k, Δu is the increment of fuel cell power ΔP_{fc}, y_1 is the SoC's change rate $\overline{SoC}$, y_2 is the mass flow $\overline{m}_{\text{H}_2}$ and T is the sample time. The cost function (12) is the cumulative hydrogen consumption, which includes the direct hydrogen consumption, the equivalent hydrogen consumption when the battery energy is used, and the penalty for the fuel cell power oscillation. Thereby, $W_{\Delta u}$ is the tuning factor with the unit of g/kW^2. It is used to penalize the oscillation of the fuel cell power. λ is the co-state derived from PMP and is used to calculate the equivalent hydrogen consumption from the battery. It has the unit of g and is updated at each time step and stays constant in the prediction horizon.

According to the requirements of the real battery and fuel cell system, the system constraints are defined as shown in Table 2.

Then, the optimization problem (12) can be formulated as a quadratic programming (QP):

$$\Delta \boldsymbol{u}_{\text{opt}} = \arg\min_{\Delta \boldsymbol{u}} \frac{1}{2} \Delta \boldsymbol{u}^T \boldsymbol{H} \Delta \boldsymbol{u} + \Delta \boldsymbol{u}^T \boldsymbol{q}, \tag{13}$$

subject to:

$$\boldsymbol{A}_{\text{ineq}} \Delta \boldsymbol{u} - \boldsymbol{b} \le 0,$$

where $\boldsymbol{H}$, $\boldsymbol{q}$, $\boldsymbol{A}_{\text{ineq}}$, $\boldsymbol{b}$ are the matrices that are rebuilt at each time step, and especially $\boldsymbol{H}$ is a positive definite matrix. Using the QP solver, the control variable can be fast calculated. The optimized result $\Delta \boldsymbol{u}_{\text{opt}}$ is a sequence of control increments, and for every time step, the control input to the vehicle model is:

$$\boldsymbol{u}(k) = \boldsymbol{u}(k-1) + \Delta \boldsymbol{u}_{\text{opt}}(k|k). \tag{14}$$

3.2. Estimation of the co-state in PMP

In PMP, the Hamiltonian function is defined as follows:

$$H(SoC, P_{fc}, \lambda, t) = \overline{m}_{H_2}(P_{fc}) + \lambda(t)\cdot\overline{SoC}(t), \tag{15}$$

where the dependence of the mass flow on the fuel cell power is already shown in Fig. 2a, and the $\lambda(t)$ represents the co-state with the same unit as that of mass. According to the optimal control theory, the dynamic of the co-state is:

$$\dot{\lambda}(t) = -\frac{\partial H(SoC, P_{fc}, \lambda, t)}{\partial SoC}. \tag{16}$$

With substituting the Hamiltonian defined in (15) into (16), the dynamics related to the co-state are expanded:

$$\dot{\lambda}(t) = -\frac{\partial \overline{m}_{H_2}}{\partial SoC} - \lambda(t)\cdot\frac{\partial \overline{SoC}}{\partial SoC} = 0 - \lambda(t)\cdot\frac{\partial \overline{SoC}}{\partial SoC}. \tag{17}$$

Because $\overline{m}_{H_2}$ is merely dependent on the control variable P_{fc}, instead of on SoC, its derivative with respect to SoC is zero.

The dynamics of the state are described in Eq. (3), with the battery current calculated in Eq. (4). From the two equations, it is evident that the battery current or rather the SoC's change rate $\overline{SoC}$ is not directly dependent on SoC. However, the open-circuit voltage and the inner resistances rely on SoC, as shown in Fig. 4. Then, the differential of the $\overline{SoC}$ to SoC is written as follows:

$$\frac{\partial \overline{SoC}}{\partial SoC} = \left(\frac{\partial \overline{SoC}}{\partial V_{oc}}\cdot\frac{\partial V_{oc}}{\partial SoC} + \frac{\partial \overline{SoC}}{\partial R_0}\cdot\frac{\partial R_0}{\partial SoC}\right), \tag{18}$$

with (17) the co-state dynamic is:

$$\dot{\lambda}(t) = -\lambda\left(\frac{\partial \overline{SoC}}{\partial V_{oc}}\cdot\frac{\partial V_{oc}}{\partial SoC} + \frac{\partial \overline{SoC}}{\partial R_0}\cdot\frac{\partial R_0}{\partial SoC}\right) \tag{19}$$

By utilization of Eqs. (3) and (4), the partial differential of $\overline{SoC}$ to V_{oc} is obtained:

$$\frac{\partial \overline{SoC}}{\partial V_{oc}} = -\frac{1}{2\cdot Q_{bat}R_0}\cdot\left(1 - \frac{V_{oc} - \sum_{i=1}^{3} V_i}{\sqrt{\left(V_{oc} - \sum_{i=1}^{3} V_i\right)^2 - 4\cdot P_{bat}\cdot R_0}}\right), \tag{20}$$

and its partial differential to R_0 is:

$$\frac{\partial \overline{SoC}}{\partial R_0} = \frac{1}{2\cdot Q_{bat}R_0^2}\left(\frac{2\cdot P_{bat}\cdot R_0 - \left(V_{oc} - \sum_{i=1}^{3} V_i\right)^2}{\sqrt{\left(V_{oc} - \sum_{i=1}^{3} V_i\right)^2 - 4\cdot P_{bat}\cdot R_0}} + \left(V_{oc} - \sum_{i=1}^{3} V_i\right)\right) \tag{21}$$

Moreover, $\frac{\partial V_{oc}}{\partial SoC}$ and $\frac{\partial R_0}{\partial SoC}$ are calculated based on the parameter curves of the battery system shown in Fig. 4.

According to PMP, the optimal control variable in each time instant minimizes the Hamiltonian:

$$P_{fc}^{*}(t) = \arg\min_{P_{fc}(t)} H(SoC, P_{fc}, \lambda, t). \tag{22}$$

Because of the monotone relation between the initial co-state and the SoC end value, a bidirectional search method, as shown in Fig. 6, can be used to determine the correct initial co-state. After the first guess of the co-state, PMP is used to determine the control variable in each discrete time point over the entire time horizon. When the iteration finishes, the current SoC end value is compared to the target value. If they are approximately identical, then the initial co-state value is found successfully, and the shooting procedure ends. If not, the initial co-state value is adjusted according to the monotone relationship between the initial co-state and the SoC end value, and the PMP iteration is repeated. The initial co-state's search range can be shorted based on a later derived formula, which estimates the co-state based on the average power and the SoC values. Thereby, the average power corresponding to the driving cycle is obtained after online simulation. The SoC used to estimate the co-state range is assumed to be 0.5 due to the charge-sustaining mode. After that, the co-state range is determined by including a ten percent derivation from the calculated value, positive and negative, respectively. It often takes less than six times iterations to realize SoC end value accuracy with four decimal digits.

As an example, the results of the offline PMP-based strategy for the driving cycle 2 (Fig. 9b) are displayed in Fig. 7, with the trajectories of SoC, the co-state and control variable included.The shooting method works to find the correct initial co-state, as the SoC end value reaches 0.5 the same as its initial value. The co-state trajectories are shown in Fig. 7b, and its amplitude in summer is lower than in winter. Since more fuel cell power is required in winter, as shown in Fig. 7a, the fuel cell system works with lower efficiency in winter than in summer, and the amplitude of co-state is correspondingly larger. In 7d, the relation of the co-state and SoC is identified, which will be derived later. Furthermore, it is evident that the fuel cell power is close to its average value. Therefore, considering the convexity of the fuel cell consumption curve in Fig. 2a, it is reasonable to assume that the differential of the Hamiltonian to control variable is zero at the average fuel cell power:

$$\left.\frac{\partial H}{\partial P_{fc}}\right|_{P_{fc}=\overline{P}_{fc}} = \left.\frac{\partial \overline{m}_{H_2}}{\partial P_{fc}} + \lambda\frac{\partial \overline{SoC}}{\partial P_{fc}}\right|_{P_{fc}=\overline{P}_{fc}} = 0, \tag{23}$$

in which, the average fuel cell power can be estimated based on the time tables of regional trains and the history information, including load and battery losses [33]. Meanwhile, the estimated average fuel cell power is used to adjust the co-state regularly when the train leaves the station. In Ref. [35], the analytical estimation of the co-state dependent on SoC and the average fuel cell power is described. In this work, the dynamics because of the R–C elements are further considered. First, the partial differential of $\overline{SoC}$ to P_{fc} can be determined from (3)(4) (6):

$$\frac{\partial \overline{SoC}}{\partial P_{fc}} = \frac{1}{Q_{bat}}\cdot\frac{1}{\sqrt{\left(V_{oc} - \sum_{i=1}^{3} V_i\right)^2 - 4\cdot P_{bat}\cdot R_0}}. \tag{24}$$

Then, the analytical formula to determine λ follows by its substitution into 23:

$$\lambda = -\frac{\partial \overline{m}_{H_2}}{\partial P_{fc}}\cdot\left(Q_{bat}\cdot\sqrt{\left(V_{oc} - \sum_{i=1}^{3} V_i\right)^2 - 4\cdot P_{bat}\cdot R_0}\right)\Bigg|_{P_{fc}=\overline{P}_{fc}}, \tag{25}$$

whereby the differential of $\overline{m}_{H_2}$ to P_{fc} can be determined using the consumption curve depicted in Fig. 2a. The dependency of V_{oc} on SoC is presented in Fig. 4. Then, assumptions have to be made for the values of V_i and the battery power. In the acceleration phases, V_i's are positive, while negative during regenerative braking. In addition, at the end of driving cycles, there is no energy stored in the polarization capacitances, which are short-circuited by their

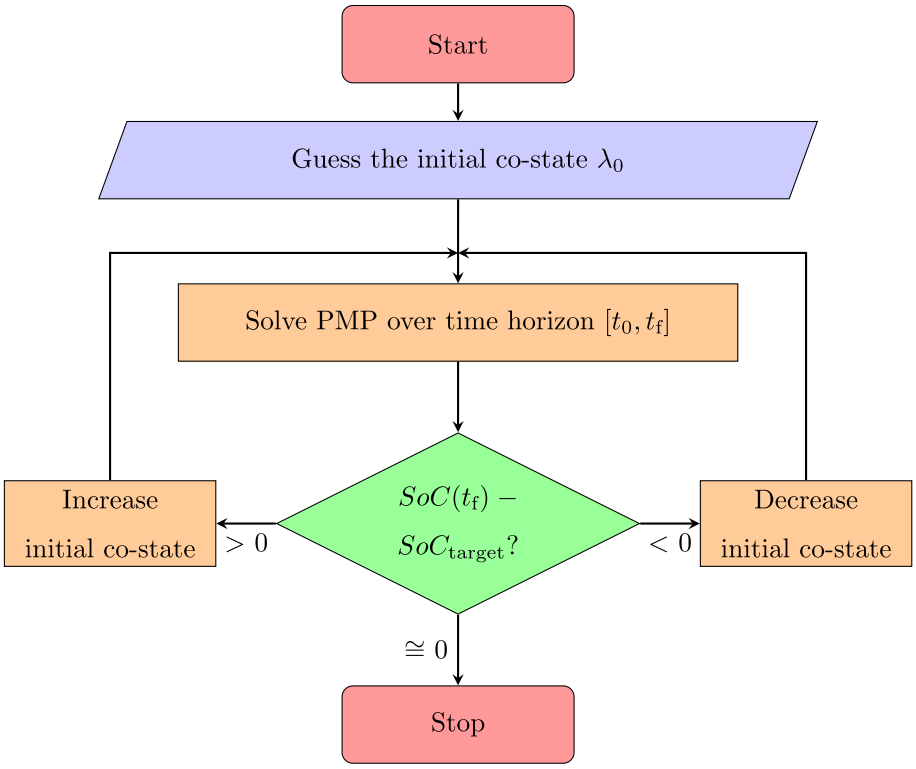

Fig. 6. Shooting method.

corresponding polarization resistances. Therefore, the values of V_i can be assumed to be zero. As the fuel cell system is operated for battery's charge-sustaining mode, the averaged battery power is zero, which is also a reasonable assumption here. Finally, an analytical formula to estimate the co-state, dependent on the averaged fuel cell power and the actual SoC, results as:

$$\lambda = -\frac{\partial \overline{m}_{H_2}}{\partial P_{fc}} \cdot Q_{bat} \cdot V_{oc,\,bat}\Big|_{P_{fc}=\overline{P}_{fc}}. \tag{26}$$

Fig. 8 shows that the analytically estimated co-state matches the resulting ones from the offline PMP strategy, which validates the estimation's correctness.

4. Simulation and analysis

The PMP-based MPC strategy is realized with MATLAB®/Simulink® and simulated in the real regional train driving cycles, as shown in Fig. 9. Driving cycle 1 represents the rail track between Aachen and Cologne, with a total distance of 70.2 km and a driving time of 3065 s. In the driving cycle 2, the rail track of Mannheim-Karlsruhe-Basel in Baden-Württemberg, with a distance of 154 km and a driving time of 8192 s, is shown.

Table 3 shows the parameters for MPC configuration. The influences of tuning factors and prediction horizon are further discussed in the subsections. To evaluate the proposed strategy, two strategies are applied for comparison. One derived from offline PMP

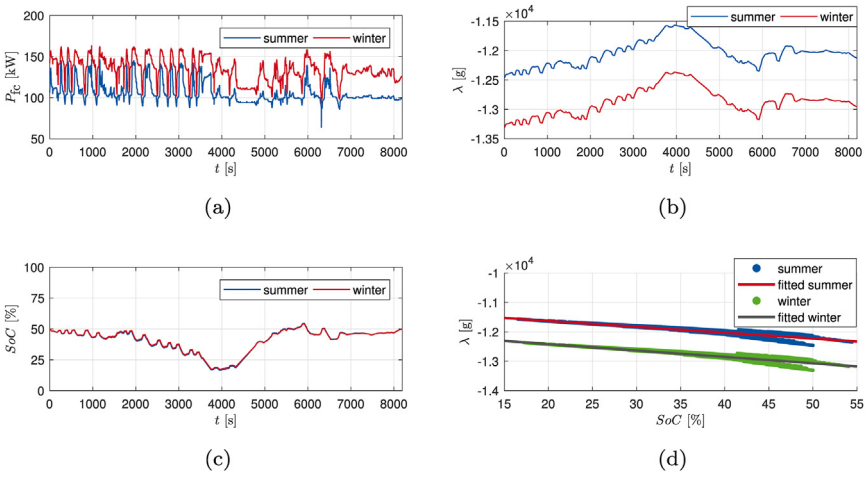

Fig. 7. Results of offline PMP-based strategy using the driving cycle 2 in summer and in winter: (a) Power of fuel cell system, (b) Co-state, (c) SoC, d) Co-state related to the SoC.

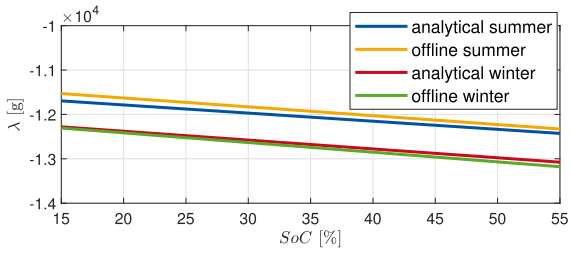

Fig. 8. Comparison of analytically estimated λ with the ones from offline results.

is used as the benchmark, while another one is a typical MPC-based strategy using the following cost function with a constant SoC reference:

$$\min_{\Delta u} J(\Delta u) = \underbrace{\sum_{i=0}^{N_u-1} \| \Delta \boldsymbol{u}(k+i|k)\|^2_{W_{\Delta \boldsymbol{u}}}}_{\text{penalty of the fuel cell power oscillation}} + \underbrace{\sum_{i=0}^{N_p} \| y_3(k+i+1|k) - y_{\text{ref}}(k+i+1|k)\|^2_{W_y}}_{\text{penalty of the battery's SoC}} + \underbrace{\sum_{i=0}^{N_p} y_2(k+i+1|k)T}_{\text{hydrogen consumption}}, \quad i = 1, \cdots, N_p - 1, \tag{27}$$

where y_{ref} is 0.5 and W_y is 10 g, which means this MPC-based strategy continually desires to hold the battery's SoC at 50%. Meanwhile, for a fair comparison, the other configurations are the same as the proposed strategy. Moreover, the strategies are simulated under both winter and summer conditions for two driving cycles and the initial SoC is set to 50%.

4.1. Simulation results and analysis

Fig. 10 shows the simulation results of the driving cycle 1. The figures in the left column correspond to the summer conditions, while the figures in the right column correspond to the winter conditions. Due to the higher power consumption of auxiliaries, the total power demand in winter is higher than in summer, which results in higher fuel cell power requirements. The second row of figures is a comparison of fuel cell power output under different strategies. Knowing the global information, the offline PMP strategy tends to keep the fuel cell output power close to 120 kW in summer and 150 kW in winter. According to Fig. 2b, the fuel cell efficiency will remain at a high level above 40%. Under the typical MPC strategy, the fuel cell power output fluctuates widely, varying from 40 kW to 180 kW. In winter due to high power demand, the fuel cell remains around 180 kW for a longer period of time than in summer, which can accelerate the degradation of the fuel cell stack [36]. In contrast, the proposed PMP-MPC strategy uses the estimated power demand based on historical data, which optimizes the fuel cell power output in a short future time. The fuel cell power is optimized to maintain around 120 kW in summer and 150 kW in winter with high efficiency like the performance of offline PMP. Furthermore, the third row of figures shows the battery's SoC for the different strategies. Despite the different power demands in winter and summer, the PMP-MPC strategy achieves to keep the SoC within a reasonable range and yields a similar result as the offline PMP strategy.

In Fig. 11, the simulation results of the driving cycle 2 are presented. Because of the long-distance and the slope characteristics of first going uphill and then going downhill, the power demand is more complicated than driving cycle 1. Due to a long-term downhill situation starting from the middle of the cycle, the typical MPC strategy has to maintain the SoC by controlling the fuel cell system at low power output, which results in low efficiency as well as the risk of acceleration degradation and reducing lifetime [36]. By comparison, the proposed PMP-MPC strategy avoids the extreme fuel cell power output and keeps the SoC within a reasonable range. Here, the final value of SoC is higher than in the previous cycle because the average power estimation is based on history and is updated every time the vehicle drives off. Therefore, the proposed strategy will adaptively adjust the power output in the next journey.

The resulting hydrogen consumptions are collected in Table 4. In summary, compared to the typical MPC strategy, the PMP-MPC strategy has achieved a significant fuel economy improvement from about 6% to 12%. Simultaneously, it also reached an optimized result with just 1.5% to 3% more hydrogen consumption than the offline PMP strategy.

4.2. Influence of tuning factors

The low fluctuation of power and the operation at part load represent an essential part of fuel cell lifetime improvement [37]. Therefore, the tuning factor $W_{\Delta \boldsymbol{u}}$ is implemented in the PMP-MPC strategy. To test the influence related to the degradation of fuel cell stacks, the tuning factors of 0.001 g/kW^2, 0.01 g/kW^2, 0.05 g/kW^2 and 0.1 g/kW^2 are applied in the strategy for driving cycle 1 in summer. The results in Fig. 12a show the fuel cell power under different tuning factors, while Fig. 12b presents the sum of absolute fuel cell power increment, from which the low fluctuation with the improving tuning factor is observed. As for hydrogen consumption shown in Table 5, the fuel economy is reduced as the tuning factor increases. Thereby, this shows a trade-off between fuel cell

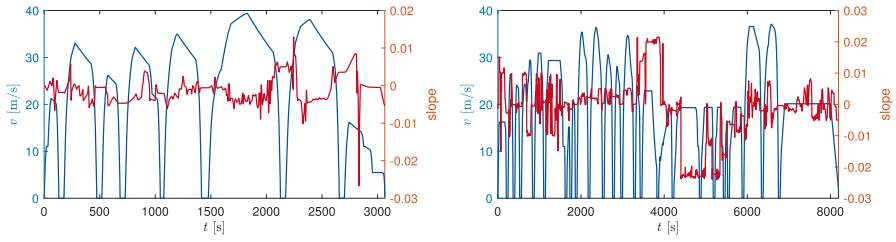

Fig. 9. Driving cycles: (a) Driving cycle 1, (b) Driving cycle 2.

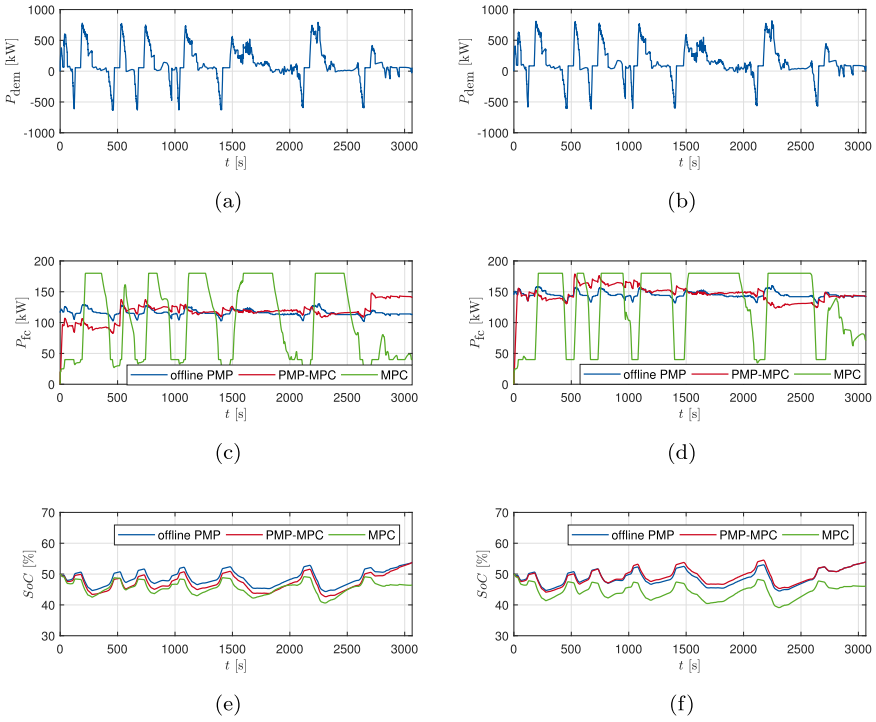

Fig. 10. Simulation results using driving cycle 1 in summer (left column) and in winter (right column): (a) (b) Power demand P_{dem} in kW, (c) (d) Power of fuel cell system P_{fc} in kW, (e) (f) SoC in %.

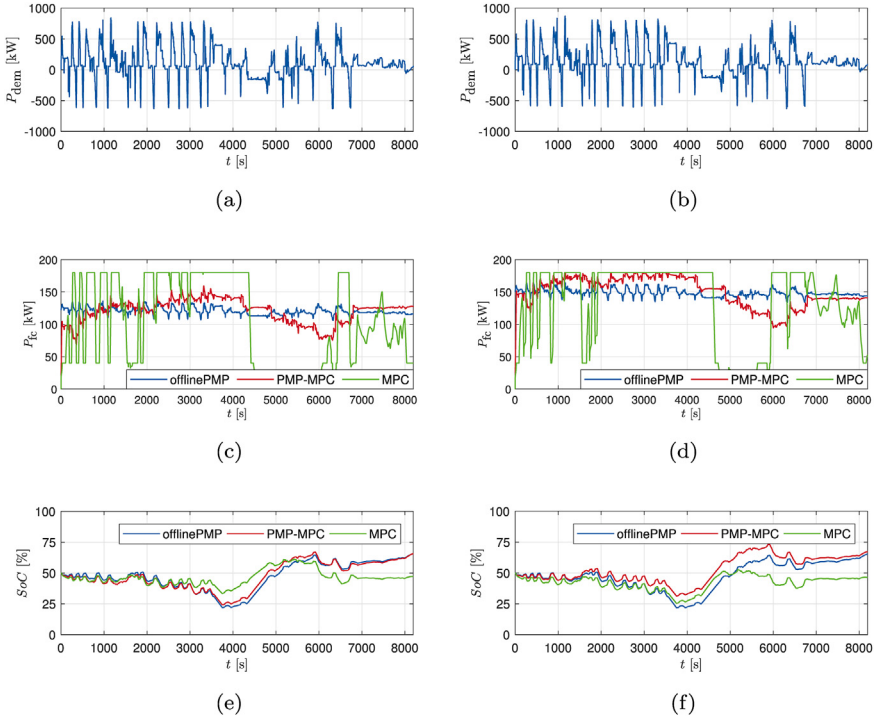

Fig. 11. Simulation results using driving cycle 2 in summer (left column) and in winter (right column): (a) (b) Power demand P_{dem} in kW, (c) (d) Power of fuel cell system P_{fc} in kW, (e) (f) SoC in %.

degradation and fuel economy. Since the core of this work is focused on fuel economy, in further tests, the tuning factor of 0.001 g/kW^2 is applied.

4.3. Influence of prediction horizon

The real-time implementation requires low computational efforts, for which the prediction horizons are changed from 10 to 40

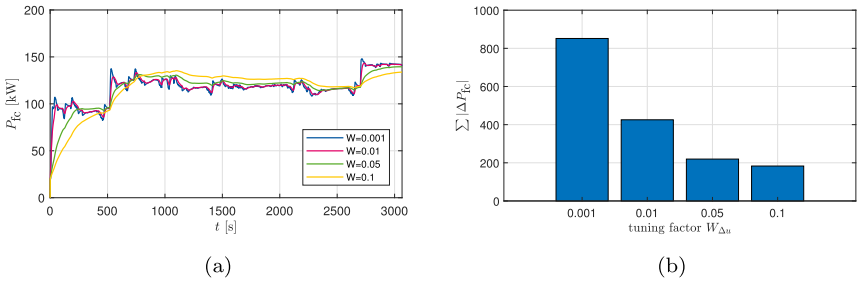

Fig. 12. Influences of tuning factors: (a) Fuel cell power profile under different tuning factors, (b) Fuel cell power oscillation under different tuning factors.

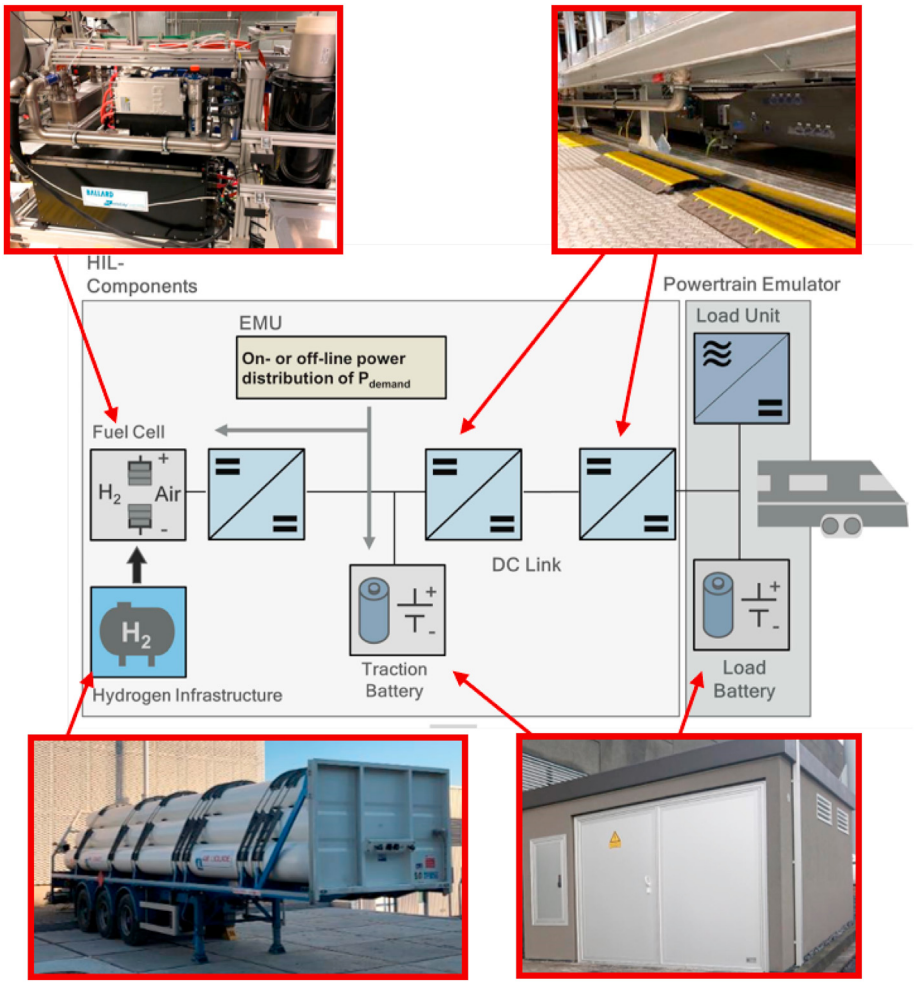

Fig. 13. Setup of HiL test bench at CMP.

steps in increments of 10 to estimate the PMP-MPC strategy in control performance and calculation time. The driving cycle 1 in summer is used for simulation, and the control horizons are simplified to be half of the prediction horizons. As Table 6 shows, the simulation time and the hydrogen consumption are trade-offs. Since the time increases significantly while the hydrogen consumption decreases slightly as the prediction horizon increases, the prediction horizon is set to 10 steps in the following tests.

5. HiL test

The simulation results have shown an excellent fuel economy of the proposed PMP-MPC strategy. Its real-time performance is evaluated and validated by a HiL test bench located at the CMP of RWTH Aachen University.

5.1. HiL setup

The central components of this test bench environment are a HiL powertrain emulator and real physical components, as shown in Fig. 13. The emulator controls the load controller to simulate the dynamic power demand that occurs in the DC link, meanwhile, it controls DC/DC converters and the fuel cell system to distribute the power flows according to power signals from energy management

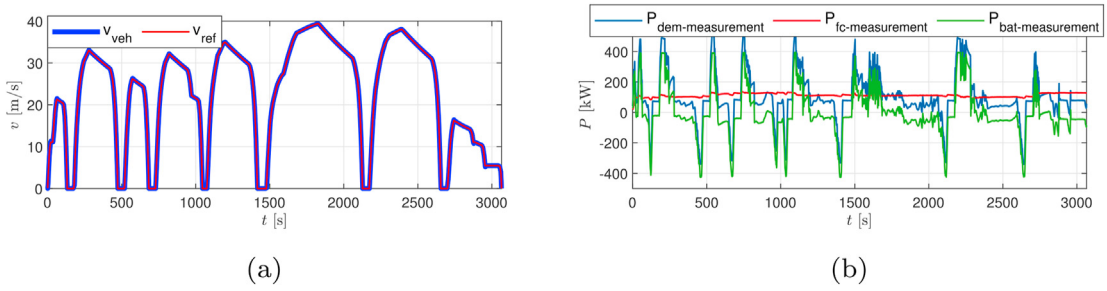

Fig. 14. HiL results using driving cycle 1 in summer with reduced-scale power: (a) Train speed v_{veh} and reference speed v_{ref} in m/s, (b) Measured reduced-scale power distribution with P_{dem}, P_{fc} and P_{bat} in kW.

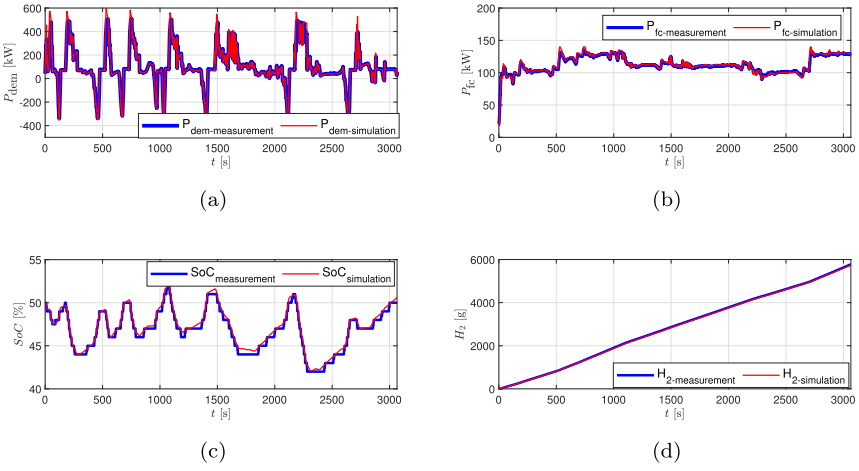

Fig. 15. HiL results using driving cycle 1 in summer with reduced-scale power: Measured and simulated value of (a) P_{dem} in kW, (b) P_{fc} in kW, (c) SoC in %, (d) H_2 in g.

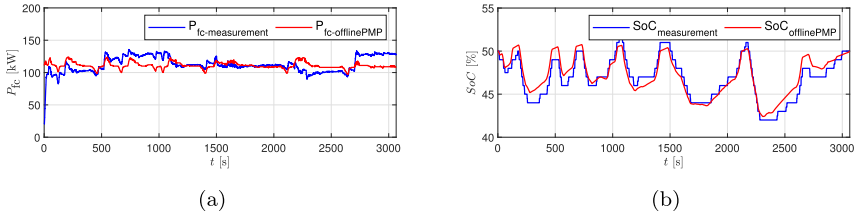

Fig. 16. Comparison between the measured results from the PMP-MPC strategy and the offline calculated global optimized results from the PMP strategy: (a) P_{fc} in kW, (b) SoC in %.

Table 2
Constraints of battery and fuel cell systems.

Min	Variable	Max
0.1	SoC	0.9
20 kW	P_{fc}	180 kW
−5 kW/s	ΔP_{fc}	5 kW/s

Table 3
MPC configuration.

Parameter	Symbol	Value
Prediction horizon	N_p	10
Control horizon	N_u	5
Tuning factor	$W_{\Delta u}$	0.001 g/kW^2
Sample time	T	1 s

system. This emulator consists of (1) a real-time system for virtual replication of the vehicle and environment model, including the auxiliaries and the energy management system, (2) measurement and control systems for coupling the virtual system with the physical components presented in the test bench.

Besides, the dSPACE SCALEXIO is used to perform the virtual systems for testing real-time behavior with the real physical components, including the DC/DC converters, battery system, fuel cell system, and a load unit. This load unit connects the supply network for compensation of additional power. In the test bench room, a second floor is built to provide a place for the systems. All DC/DC converters are positioned on the test bench foundation due to their high weight, while the fuel cell system with rated net power of 200 kW is installed above on the second floor. Outside of the test field, the hydrogen supply is ensured by hydrogen trailers with a capacity of approx. 350 kg hydrogen, which guarantees endurance testing over period of several days. Moreover, the battery systems are placed in a garage concerning safety precautions.

Table 4
Simulation results of different strategies.

Cycles	Strategies	SoC_{end}[%]	H_2[g]	Equiv. H_2[g]	Difference[%]
1, winter	offline PMP	54.01	7923.8	7378.6	−1.7
1, winter	PMP-MPC	54.01	8051.7	7505.1	0
1, winter	MPC	46.12	7485.1	8013.9	6.8
1, summer	offline PMP	53.78	5939.9	5456.7	−1.5
1, summer	PMP-MPC	53.78	6057.6	5542.4	0
1, summer	MPC	46.45	5718.2	6202.1	11.9
2, winter	offline PMP	67.35	21868	19461.9	−3
2, winter	PMP-MPC	67.36	22467	20059.5	0
2, winter	MPC	46.34	20636	21143.6	5.4
2, summer	offline PMP	65.77	16322	14135	−3
2, summer	PMP-MPC	65.77	16764	14577	0
2, summer	MPC	47.22	15949	16334.5	12.1

Table 5
Simulation results using different tuning factors.

Tuning factors[g/kW^2]	SoC_{end}[%]	H_2[g]	Equiv. H_2[g]	Difference[%]
0.001	53.78	6057.6	5542.3	0
0.01	53.74	6052.3	5542.5	0.003
0.05	53.51	6044	5565.5	0.418
0.1	53.32	6051.2	5598.6	1.015

During the HiL test, the driver model and the driveline model simulate the power demand. The power demand is implemented by the load side DCDC converter on the test bench. At the same time, the MPC energy management controller predicts the states based on the measured data, and generates the desired fuel cell power by minimizing the cost function. The fuel cell system on the test bench outputs the power following the determined value by energy management. A source side DCDC converter controls the voltage of the DC link. Then, the battery system on the test bench compensates the rest power to fulfill the power demand. In addition to the real systems on the test bench, the fuel cell and battery models are running simultaneously. The measured fuel cell power is fed into the fuel cell model to calculate hydrogen consumption. The measured battery power is sent to the battery model to simulate the battery behavior.

Due to technical issues, the system's power is restricted, and the following sets are made to downscale power: (1) Two of the three branches of traction battery are used while the simulated battery power is scaled to two third of the original power. (2) The maximum fuel cell power output of the model is limited to 140 kW. (3) The total passenger number is reduced from 120 to 60. Then, the driving cycle 1 in summer is used to perform the HiL tests.

5.2. HiL results

In Fig. 14 the results of speed tracking and the measured power distribution are presented. As displayed in Fig. 14a, the vehicle speed matches the reference speed. The measured power distribution in Fig. 14b shows that the fuel cell power covers the average load power and the battery system provides the peak power.

Fig. 15 shows the various measured and simulated trajectories under the PMP-MPC strategy. In Fig. 15a, the power demand is satisfied without being restricted by the battery or fuel cell system. The tiny differences between the measured and simulated power demand can be found because of the limited power ramp in the power electronics. In Fig. 15b, the measured fuel cell power has a negligible deviation from the simulated fuel cell power. Meanwhile, the fuel cell power is maintained at around 110 kW with high efficiency, which covers the average load power. Fig. 15c shows an overlapping between the measured and simulated battery's SoC. The measured end SoC is 50% and the simulated end SoC is 50.67%, which proves the correctness of battery modeling and shows the good charge sustaining under the PMP-MPC strategy. Moreover in Fig. 15d, the simulated hydrogen consumption is 5733.3 g and the measured one is 5778.7 g. The deviation of 0.8% shows that the correctness of the specific consumption curve of the fuel cell system is validated.

Table 7
Comparison between the measured hydrogen consumption under the PMP-MPC strategy and the offline calculated hydrogen consumption from the PMP strategy.

Strategies	SoC_{end}[%]	H_2[g]	Difference[%]
offline PMP	50	5625.9	0
PMP-MPC	50	5778.7	+2.7

To evaluate the fuel economy of the PMP-MPC strategy, the global optimized results from the offline PMP strategy are used. As the fuel cell system and the battery system modeling are validated, the measured fuel cell and battery power are summed and used as inputs for offline PMP. The offline calculated optimal trajectories of the fuel cell power and SoC are displayed in Fig. 16. It can be pointed out, the averaged fuel cell power from the PMP-MPC is close to the one from the offline PMP. Due to the start-up process of the fuel cell system and the lack of global information, the trajectories of PMP-MPC have deviations compared to the offline PMP, as shown in Fig. 16a. With the same end SoC of 50% in Fig. 16b, the offline calculated hydrogen consumption is 5625.9 g, which is about 2.7% less than the measured hydrogen consumption from the PMP-MPC strategy. In summary, a comparison of the PMP-MPC strategy and offline PMP strategy regarding the HiL tests is shown in Table 7.

6. Conclusions

In this work, an adaptive PMP-based MPC strategy for fuel cell hybrid railway vehicles is proposed. Under the framework of MPC, the strategy can handle strict constraints on control and state variables. First, a linear time-varying model under consideration of battery modeling with three R–C elements is formulated. For the fuel economy and battery's charge sustaining, the co-state derived in PMP is used to formulate the cost function. The calculation and update of the co-state depend on a quantitative analytical formula, which utilizes characteristic curves of source components. Then, the performance of the strategy is tested in simulation for two real driving cycles in summer and winter, and compared with the offline PMP and a typical MPC strategy. The simulation results show that proposed PMP-based MPC strategy provides significant

Table 6
Influence of different prediction horizons.

Prediction horizon	SoC_{end}[%]	H_2[g]	Equiv. H_2[g]	Difference[%]	Simulation time of driving cycle 1 [s]
10	53.78	6057.6	5542.3	0	372
20	53.77	6054.5	5540.6	−0.03	566
30	53.75	6051.1	5539.9	−0.04	740
40	53.74	6048.7	5538.9	−0.06	987

improvement of about 12.1% in fuel economy than the typical MPC strategy and also it provides sub-optimal solution close to offline PMP strategy. Besides that, the influence of the tuning factor and prediction horizon concerning the fuel cell degradation, computational effort, and hydrogen consumption are presented. Finally, the proposed strategy is implemented on a HiL test bench located at the CMP of RWTH Aachen University with high power fuel cell and battery systems, from which an excellent real-time performance with merely 2.7% more hydrogen consumption than the global optimum is observed.

References

[1] Study on the use of fuel cells & hydrogen in the railway environment, report 2: analysis of boundary conditions for potential hydrogen rail applications of selected case studies in europe. https://shift2rail.org/wp-content/uploads/2019/04/Report-2.pdf. [Accessed 29 June 2020].

[2] Study on the use of fuel cells & hydrogen in the railway environment, report 1: state of the art & business case and market potential. https://shift2rail.org/wp-content/uploads/2019/04/Report-1.pdf. [Accessed 29 June 2020].

[3] Railway statistics report. https://uic.org/IMG/pdf/synopsis_2015_print_5_.pdf. [Accessed 29 June 2020].

[4] Coradia ilint – the world's 1st hydrogen powered train. https://www.alstom.com/our-solutions/rolling-stock/coradia-ilint-worlds-1st-hydrogen-powered-train. [Accessed 29 June 2020].

[5] Siemens receives funding approval for development of fuel cell drive for trains. https://www.now-gmbh.de/en/news/press/Siemens-receives-funding-approval-for-development-of-fuel-cell-drive-for-trains. [Accessed 29 June 2020].

[6] Xu N, Kong Y, Chu L, Ju H, Yang Z, Xu Z, Xu Z. Towards a smarter energy management system for hybrid vehicles: a comprehensive review of control strategies. Appl Sci 2019;9(10):2026.

[7] Ali AM, Söffker D. Towards optimal power management of hybrid electric vehicles in real-time: a review on methods, challenges, and state-of-the-art solutions. Energies 2018;11(3):476.

[8] Banvait H, Anwar S, Chen Y. A rule-based energy management strategy for plug-in hybrid electric vehicle (phev). In: 2009 American control conference. IEEE; 2009. p. 3938–43.

[9] Gao D, Jin Z, Lu Q. Energy management strategy based on fuzzy logic for a fuel cell hybrid bus. J Power Sources 2008;185(1):311–7.

[10] Zhou H, Xu Z, Liu L, Liu D, Zhang L. A rule-based energy management strategy based on dynamic programming for hydraulic hybrid vehicles. Mathematical Problems in Engineering 2018;2018:10. https://doi.org/10.1155/2018/9492026. 9492026.

[11] Peng J, He H, Xiong R. Rule based energy management strategy for a series–parallel plug-in hybrid electric bus optimized by dynamic programming. Appl Energy 2017;185:1633–43.

[12] Bellman R. The theory of dynamic programming. Bull Am Math Soc 1954;60(6):503–15.

[13] Peng H, Li J, Deng K, Thul A, Li W, Lowenstein L, Sauer DU, Hameyer K. An efficient optimum energy management strategy using parallel dynamic programming for a hybrid train powered by fuel-cells and batteries. In: 2019 IEEE vehicle power and propulsion conference. VPPC); 2019. p. 1–7.

[14] Xu L, Ouyang M, Li J, Yang F, Lu L, Hua J. Application of pontryagin's minimal principle to the energy management strategy of plugin fuel cell electric vehicles. Int J Hydrogen Energy 2013;38(24):10104–15.

[15] Rezaei A, Burl JB, Zhou B. Estimation of the ecms equivalent factor bounds for hybrid electric vehicles. IEEE Trans Contr Syst Technol 2017;26(6):2198–205.

[16] Park J, Park J-H. Development of equivalent fuel consumption minimization strategy for hybrid electric vehicles. Int J Automot Technol 2012;13(5):835–43.

[17] D. Pei, M. J. Leamy, Dynamic programming-informed equivalent cost minimization control strategies for hybrid-electric vehicles, J Dyn Syst Meas Contr 135 (5).

[18] Tian X, Cai Y, Sun X, Zhu Z, Xu Y. An adaptive ecms with driving style recognition for energy optimization of parallel hybrid electric buses. Energy 2019;189:116151.

[19] Zhang P, Yan F, Du C. A comprehensive analysis of energy management strategies for hybrid electric vehicles based on bibliometrics. Renew Sustain Energy Rev 2015;48:88–104.

[20] Xie S, Hu X, Xin Z, Brighton J. Pontryagin's minimum principle based model predictive control of energy management for a plug-in hybrid electric bus. Appl Energy 2019;236:893–905.

[21] Uebel S, Murgovski N, Bäker B, Sjöberg J. A two-level mpc for energy management including velocity control of hybrid electric vehicles. IEEE Trans Veh Technol 2019;68(6):5494–505.

[22] Zhang Y, Chu L, Ding Y, Xu N, Guo C, Fu Z, Xu L, Tang X, Liu Y. A hierarchical energy management strategy based on model predictive control for plug-in hybrid electric vehicles. IEEE Access 2019;7:81612–29.

[23] Zhou Y, Li H, Ravey A, Péra M-C. An integrated predictive energy management for light-duty range-extended plug-in fuel cell electric vehicle. J Power Sources 2020;451:227780.

[24] He H., Quan S., Sun F., Wang Y. Model Predictive Control With Lifetime Constraints Based Energy Management Strategy for Proton Exchange Membrane Fuel Cell Hybrid Power Systems," in. IEEE Transactions on Industrial Electronics Oct. 2020;67(10):9012–9023.

[25] Hu X, Zou C, Tang X, Liu T, Hu L. Cost-optimal energy management of hybrid electric vehicles using fuel cell/battery health-aware predictive control. IEEE Trans Power Electron 2019;35(1):382–92.

[26] Li L, Coskun S, Zhang F, Langari R, Xi J. Energy management of hybrid electric vehicle using vehicle lateral dynamic in velocity prediction. IEEE Trans Veh Technol 2019;68(4):3279–93.

[27] Li X, Wang Y, Yang D, Chen Z. Adaptive energy management strategy for fuel cell/battery hybrid vehicles using pontryagin's minimal principle. J Power Sources 2019;440:227105.

[28] Hou J, Song Z. A hierarchical energy management strategy for hybrid energy storage via vehicle-to-cloud connectivity. Appl Energy 2020;257:113900.

[29] Du G, Zou Y, Zhang X, Kong Z, Wu J, He D. Intelligent energy management for hybrid electric tracked vehicles using online reinforcement learning. Appl Energy 2019;251:113388.

[30] Liu B, Wang T, Wang H, Li L. Nonlinear model predictive control for series-parallel hybrid electric buses. IEEE Access 2019;7:138792–802.

[31] Wang H, Huang Y, Khajepour A, Song Q. Model predictive control-based energy management strategy for a series hybrid electric tracked vehicle. Appl Energy 2016;182:105–14.

[32] Xie S, He H, Peng J. An energy management strategy based on stochastic model predictive control for plug-in hybrid electric buses. Appl Energy 2017;196:279–88.

[33] Peng H, Li J, Thul A, Deng K, Ünlübayir C, Löwenstein L, Hameyer K. A scalable, causal, adaptive rule-based energy management for fuel cell hybrid railway vehicles learned from results of dynamic programming. eTransportation 2020:100057.

[34] Ihme J. Fahrwiderstände von schienenfahrzeugen. In: Schienenfahrzeugtechnik. Springer; 2019. p. 31–49.

[35] Peng H, Li J, Löwenstein L, Hameyer K. A scalable, causal, adaptive energy management strategy based on optimal control theory for a fuel cell hybrid railway vehicle. Appl Energy 2020;267:114987.

[36] Chen H, Pei P, Song M. Lifetime prediction and the economic lifetime of proton exchange membrane fuel cells. Appl Energy 2015;142:154–63.

[37] Fletcher T, Thring R, Watkinson M. An energy management strategy to concurrently optimise fuel consumption & pem fuel cell lifetime in a hybrid vehicle. Int J Hydrogen Energy 2016;41(46):21503–15.